Mechanical Stability of Mesoporous Molecular Sieve MCM-48 Studied by Adsorption of Benzene, *n*-Heptane, and Cyclohexane

Martin Hartmann* and Christian Bischof

Institute of Chemical Technology I, University of Stuttgart, D-70550 Stuttgart, Germany

Received: March 30, 1999; In Final Form: June 2, 1999

The synthesis of MCM-48 has been performed in a 5 L autoclave, and the progress of the synthesis has been monitored by X-ray powder diffraction and ^{29}Si MAS NMR. The formation of MCM-48 progresses via an intermediate phase, whose conversion into the cubic phase is triggered by condensation of the silanol groups. The mechanical stability of silica mesoporous material MCM-48 has been investigated employing powder X-ray diffraction, nitrogen adsorption, and subcritical organic vapor (benzene, *n*-heptane, and cyclohexane) adsorption isotherms and breakthrough curves. The adsorption capacity is affected considerably by mechanical compression between 20 and 400 N mm^{-2}, while the material is destroyed to a large extend at 480 and 600 N mm^{-2}, which is reflected by a dramatic decrease in adsorption capacity and poor X-ray diffraction patterns. As a result of its three-dimensional structure, the mechanical stability of MCM-48 is larger compared to that of MCM-41 but still low compared to that of crystalline structures such as zeolites.

Introduction

Since the discovery of ordered mesoporous molecular sieves with pore sizes between 2 and 10 nm, much research work has been devoted to this new class of materials, denoted M41S. However, most studies focused on the hexagonal member of this group, MCM-41.[1] The same synthesis principle can be applied for the synthesis of another member of this family, the cubic phase MCM-48, although only little information is available on the synthesis and the properties of this material.[2−4] However, MCM-48 with its three-dimensional channel system seems more attractive for catalytic applications than MCM-41, which possesses a one-dimensional arrangement of channels. It is reasonable to assume that MCM-48 is more resistant to deactivation due to pore blocking.

While nitrogen adsorption data are published in almost every paper dealing with the M41S family of materials, studies on adsorption of organics in MCM-41 and MCM-48 are very limited. Vartuli et al. determined the adsorption capacities for benzene in MCM-41 and MCM-48 and obtained values up to 0.66 and 0.55 kg/kg, respectively.[5] The benzene sorption capacities of Co/MCM-41 and MCM-41 were compared by Jentys et al. and found to be slightly different.[6] Zhao and Lu compared benzene adsorption in MCM-41 before and after silylation and concluded that the pore configuration effects the adsorption while the surface chemistry plays only a minor role.[7] The adsorption of benzene in MCM-41 materials with different pore sizes was studied by Nguyen et al.[8] and Inagaki et al.[9] Rathousky et al. investigated the adsorption of cyclopentane at temperatures between 243 and 333 K and obtained maximum loadings of 0.53 kg/kg.[10] Chen et al.[11] compared cyclohexane sorption on MCM-41 and Al−MCM-41 and found maximum adsorption capacities of 0.5 and 0.45 kg/kg, respectively. Only a slight influence of the aluminum content on the adsorptive properties of MCM-41 has also been found by Boger et al.[12] using toluene as a probe molecule. The *n*-hexane adsorption capacity was determined by Hansen et al. to be 0.55 kg/kg.[13] The adsorption isotherms of cyclohexane were studied by Long et al. to investigate the adsorption behavior of MCM-41 and trimethylsilylated MCM-41.[14] The adsorption of *n*-hexane, toluene, and acetonitrile onto aluminum-containing MCM-41 has also been recently reported by Jänichen et al.[15,16] All data reported so far show that the pore volume accessible for subcritical organic vapors and, hence, the adsorption capacity are large and typically in excess of 0.5 kg/kg. However, there is a lack of those studies for MCM-48.

Mechanical stability is an important characteristic of an adsorbent or catalyst for most practical applications. Prior to adsorption or catalytic studies or IR or electric conductivity measurements, the amorphous powders obtained by hydrothermal synthesis are usually compacted at high pressures into pellets. They are also routinely subjected to high pressure for preparation and use as a chromatographic column (HPLC) packing and extrusion along with a binder for industrial process application.

Envisaging large-scale industrial applications of these molecular sieves, two major questions have only been scarcely addressed: can these materials be produced on a larger scale and can they withstand mechanical stress during a shaping process? Therefore, in this study, MCM-48 has been synthesized in a 5 L autoclave and the mechanical stability has been studied by pelletization employing different pressures and subsequent adsorption of benzene, cyclohexane, and *n*-heptane under static and flow conditions. The results have been compared with nitrogen adsorption data and powder X-ray diffraction patterns.

Experimental Section

Synthesis. Mesoporous all-silica MCM-48 was synthesized in a 5 L autoclave using hexadecyltrimethylammoniumbromide (C_{16}TAB, Aldrich), tetraorthosilicate (TEOS, Aldrich), and diluted NaOH. First, a gel with the molar composition n_{Si}/n_{CTAB}/

* To whom correspondence should be addressed. Present address: Department of Chemistry, Chemical Technology, University of Kaiserslautern, P.O. Box 3049, D-67653 Kaiserslautern, Germany. Fax: +49-631-205-4193. E-mail: hartmann@rhrk.uni-kl.de.

10.1021/jp991103a CCC: $18.00
Published on Web 07/14/1999

n_{Na_2O}/n_{H_2O} = 1.0:0.6:0.5:63 was prepared. A typical synthesis procedure is outlined as follows. First, 840 g of hexadecyltrimethylammoniumbromide (C_{16}TAB) was diluted in 2.5 L of distilled water under stirring at 50 °C to give a 25 wt % solution. Then, 800 g of TEOS was slowly added and the resultant solution was stirred for 5 min. After addition of 1.25 L of a 1 M NaOH solution, the gel was stirred for another 5 min. Thereafter, the resultant synthesis gel was charged into a 5 L autoclave and heated to 100 °C under agitation. To monitor the progress in MCM-48 formation, small samples were taken every 2 h from the autoclave. Each sample was washed with 100 mL of ethanol and 250 mL of distilled water and subsequently dried at 80 °C for 24 h to secure comparable conditions for further characterizations. After 40 h, the synthesis was stopped and the resultant material was filtered, washed with ethanol and water, and air-dried. To remove the surfactant, the as-synthesized material was calcined for 10 h at 540 °C in a flow of nitrogen and, thereafter, air.

Characterization. The chemical composition of the samples was determined by atomic adsorption spectroscopy (AAS). X-ray powder diffraction patterns were recorded after synthesis and template removal on a Siemens D5000 diffractometer using Cu Kα radiation. After calcination, nitrogen adsorption and desorption isotherms were measured at 77 K on a Micromeritics ASAP 2010 sorption analyzer. The specific surface area was obtained using the standard BET method, while pore volume and pore size distribution were calculaled by employing the Barrett−Joyner−Halenda (BJH) formalism from the desorption isotherm. ^{29}Si MAS NMR spectra were recorded on a Bruker MSL 400 spectrometer using single-pulse excitation with standard 7 mm rotors. The resonance frequency was $\omega_0/2\pi$ = 79.49 MHz. Tetramethylsilane (TMS) was employed as the chemical shift reference.

Pelletizing. To test the mechanical stability of MCM-48, the samples were compressed in a steel die of 40 mm diameter, using a hand-operated press, for 30 min. The six different external pressures applied (20, 80, 240, 400, 480, and 600 N mm^{-2}) were calculated from the external force and the diameter of the die. Subsequently, the obtained disk was crushed and sieved to obtain pellets with a diameter of 0.2 to 0.3 mm, which were used for all further measurements.

Adsorption. At room temperature (T_{ads} = 21 °C) benzene, *n*-heptane, and cyclohexane adsorption isotherms were measured using a home-built system consisting of a CAHN D200 microbalance connected to a high-vacuum system. With each adsorptive, adsorption equilibrium was achieved within 20 min, apart from the steep middle region of the isotherm, where up to 90 min was required for equilibration. The breakthrough experiments (T_{ads} = 45 °C) were conducted under atmospheric pressure in a flow-type apparatus with a fixed-bed reactor, saturator, and on-line capillary gas chromatograph. Prior to the adsorption experiments, the samples were dehydrated at 200 °C in a vacuum ($p < 10^{-5}$ hPa) or in a nitrogen flow (V/t = 50 cm^3 min^{-1}).

Results

Figure 1 exhibits the X-ray diffraction patterns for a MCM-48 synthesis batch as a function of the reaction time in a 5 L autoclave. For a better view, the diffraction patterns of samples taken every 4 h were displayed. Hence, it appears that the formation of the MCM-48 structure is completed after 22 h. No further increase in the X-ray diffraction intensity is observed between 22 and 40 h, but a lamellar phase starts to appear thereafter. Between 6 and 18 h of the reaction time, a broad reflection is observed at 2θ = 3.7°. With increasing synthesis time, this signal becomes lower in intensity, indicating that the cubic MCM-48 is probably built over an intermediate phase.[4]

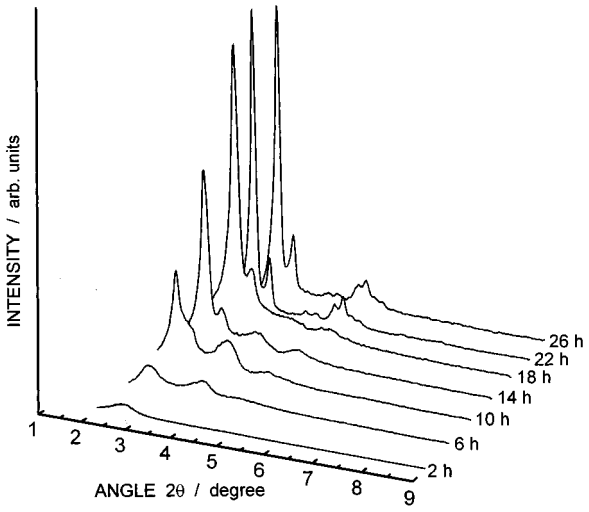

Figure 1. Powder X-ray diffraction patterns of samples taken from a MCM-48 synthesis batch after different reaction times.

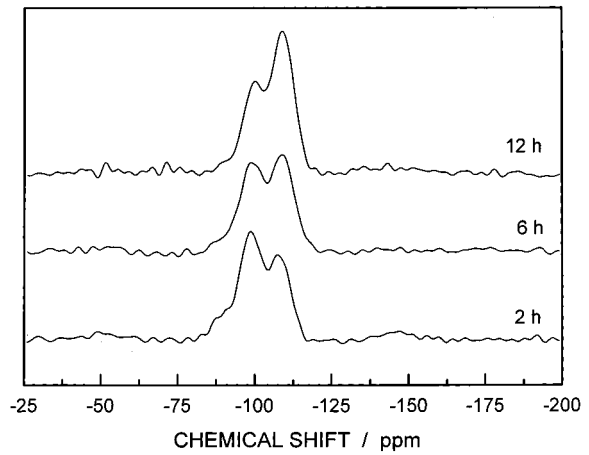

Figure 2. ^{29}Si MAS NMR spectra of as-synthesized MCM-48 samples after different synthesis times.

The ^{29}Si MAS NMR spectra of the as-synthesized samples (Figure 2) show that during the synthesis of the MCM-48 condensation of the silanol groups takes place. The Q^4/Q^3 ratio increases with increasing reaction time. The Q^4/Q^3 ratio in the synthesis gel (t = 0) is 0.93, and after a reaction time of 12 h the Q^4/Q^3 ratio has increased to 1.58.

The powder X-ray diffraction patterns of the pressed MCM-48 are displayed in Figure 3. The quality of the pattern decreases only slightly with increasing pelletizing pressure up to 400 N mm^{-2}, while the structural information is lost for pressures higher than 480 N mm^{-2}. The (211), (220), and higher reflections did not shift considerably, which indicates no significant changes of the MCM-48 unit cell.

In Table 1, the results of the nitrogen adsorption and desorption measurements are summarized. With increasing pelletizing pressure pore volume V_p and BET surface area decrease, while the pore diameter derived from application of the BJH method is virtually unaffected. The theoretical basis for the BJH analysis becomes fairly weak for our systems, where the step is at p/p_0 = 0.25, which is below the stabilization limit of the meniscus (p/p_0 = 0.42).[17] Also, the assumption of cylindrical pores is not without problems, considering the interwowen three-dimensional pore system of MCM-48. How-

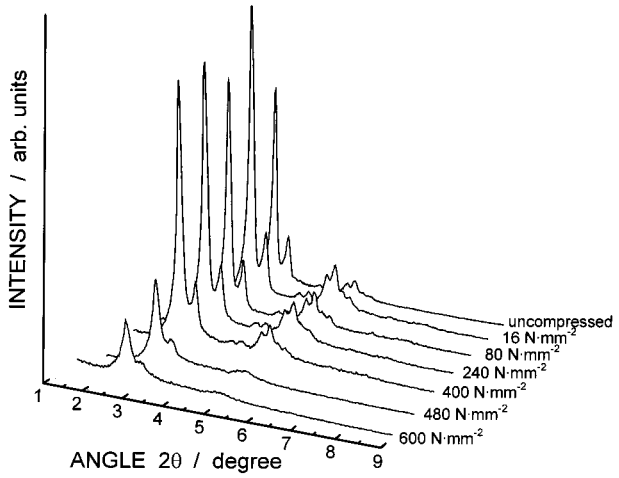

Figure 3. Powder XRD patterns of MCM-48 materials after application of external forces to form pellets.

TABLE 1: Results of the Nitrogen Adsorption Isotherms at 77 K

sample	pressure (N mm^{-2})	BET surface (m^2 g^{-1})	pore volume (cm^3 g^{-1})	pore diameter (nm)
MCM-48-(20)	20	1240	1.01	2.3
MCM-48-(80)	80	1220	0.98	2.4
MCM-48-(240)	240	1080	0.80	2.3
MCM-48-(400)	380	1060	0.75	2.3
MCM-48-(480)	480	900	0.59	2.1
MCM-48-(600)	600	720	0.39	(1.9)

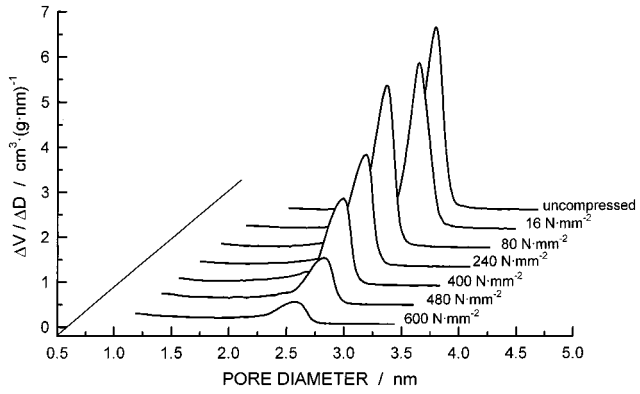

Figure 4. Pore size distributions of MCM-48 calculated from the BJH model after compression at different pressures.

ever, pore sizes calculated are still probably in the right range.[17] The mean pore diameter calculated for our samples is ca. 2.3 nm, which is typical for MCM-48 materials synthesized with C_{16}TAB as a surfactant.[3] The pore diameter distribution is only slightly broadened as shown in Figure 4, which indicates only minimal pore deformation upon compression. The ordered porous structure of the sample is destroyed to a large extend at 600 N/mm^2, as indicated by the rather small pore volume of 0.39 cm^3 g^{-1}.

In Figure 5, the breakthrough curves of benzene over the pressed MCM-48 materials are depicted. After $t = 40$ min, benzene breaks through almost independently of the compression pressure. Once benzene appears, its partial pressure at the adsorber outlet increases rapidly until $p_{\text{benzene}}/p_{\text{benzene},0} = 0.8$, where it reaches a plateau. The length of this plateau depends on the time necessary to achieve complete filling of the pores by capillary condensation. The breakthrough curves of cyclohexane at 45 °C and partial pressure $p_{\text{cyclohexane},0} = 63$ hPa are displayed in Figure 6. After 20 min on stream, cyclohexane breaks through and reaches a plateau at $p_{\text{cyclohexane}}/p_{\text{cyclohexane},0} = 0.85$. *n*-Heptane ($p_{n-\text{heptane},0} = 44.9$ hPa) breaks through after 25 min on stream and reaches the plateau at $p_{n-\text{heptane}}/p_{n-\text{heptane}} = 0.4$ (Figure 7). The length of the plateau increases with decreasing pelletizing pressure, which indicates a greater pore-filling capacity. In Table 2, the loadings of benzene, *n*-heptane, and cyclohexane derived from the breakthrough curves and the corresponding calculated pore volumes are summarized. For the calculation of the pore volumes, the density of the adsorbed organics was assumed to be that of the bulk liquid at adsorption temperature ($T = 45$ °C). The obtained values are consistently

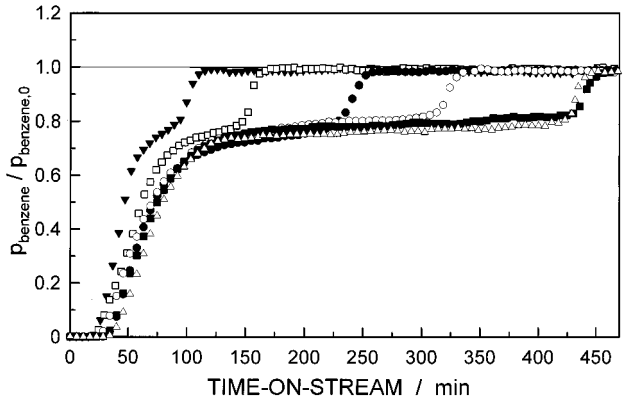

Figure 5. Breakthrough curves at 45 °C for benzene on MCM-48 pelletized at different pressures: (■) MCM-48-(20); (△) MCM-48-(80); (○) MCM-48-(240); (●) MCM-48-(400); (□) MCM-48-(480); (▼) MCM-48-(600).

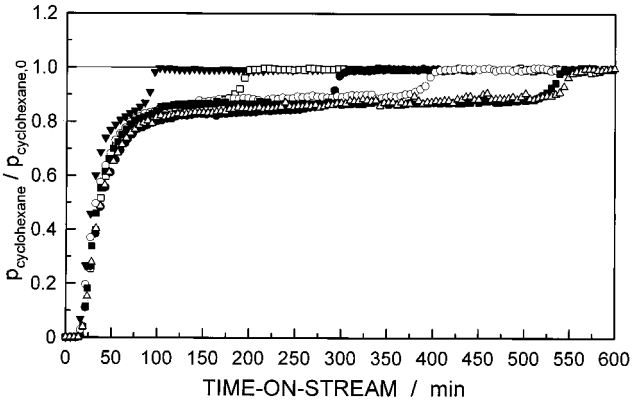

Figure 6. Breakthrough curves at 45 °C for cyclohexane on MCM-48 pelletized at different pressures: (■) MCM-48-(20); (△) MCM-48-(80); (○) MCM-48-(240); (●) MCM-48-(400); (□) MCM-48-(480); (▼) MCM-48-(600).

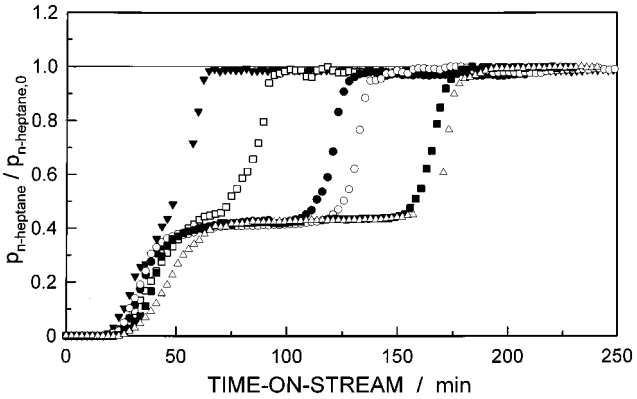

Figure 7. Breakthrough curves at 45 °C for *n*-heptane on MCM-48 pelletized at different pressures: (■) MCM-48-(20); (△) MCM-48-(80); (○) MCM-48-(240); (●) MCM-48-(400); (□) MCM-48-(480); (▼) MCM-48-(600).

TABLE 2: Adsorption of Benzene, *n*-Heptane, and Cyclohexane Calculated from the Breakthrough Curves at 45 °C

		benzene		*n*-heptane		cyclohexane	
pelletizing pressure (N mm^{-2})	V_p (N_2) (cm^3 g^{-1})	n_{ads} (mmol g^{-1})	V_{calc} (cm^3 g^{-1})	n_{ads} (mmol g^{-1})	V_{calc} (cm^3 g^{-1})	n_{ads} (mmol g^{-1})	V_{calc} (cm^3 g^{-1})
20	1.01	9.8	0.90	5.4	0.81	7.3	0.81
80	0.98	9.7	0.89	5.3	0.80	7.3	0.81
240	0.80	7.7	0.71	4.1	0.62	5.8	0.65
400	0.75	6.9	0.63	3.8	0.57	5.2	0.58
480	0.59	5.3	0.49	2.8	0.42	3.7	0.41
600	0.39	3.8	0.35	2.0	0.30	2.5	0.28

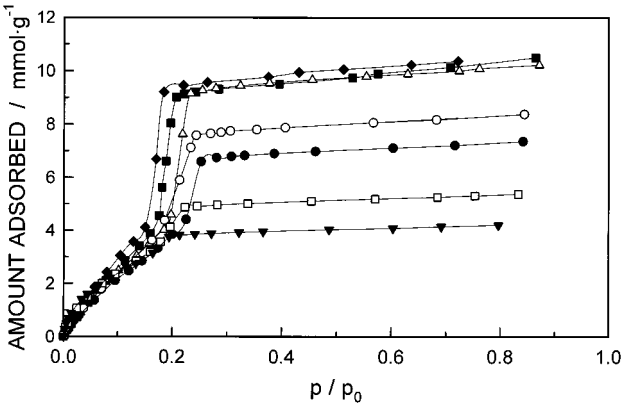

Figure 8. Benzene adsorption isotherms at 21 °C on MCM-48: (◆) uncompressed sample; (■) MCM-48-(20); (△) MCM-48-(80); (○) MCM-48-(240); (●) MCM-48-(400); (□) MCM-48-(480); (▼) MCM-48-(600).

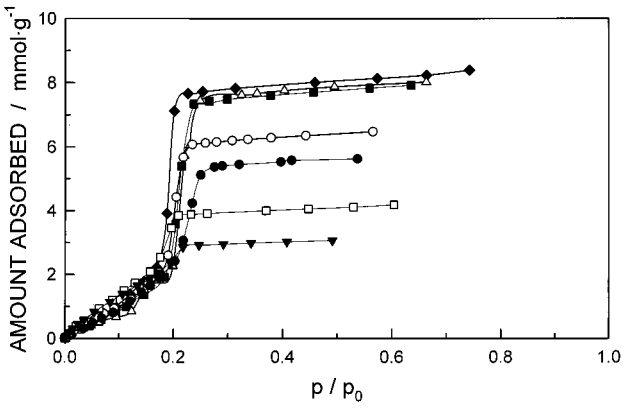

Figure 9. Cyclohexane adsorption isotherms at 21 °C on MCM-48: (◆) uncompressed sample; (■) MCM-48-(20); (△) MCM-48-(80); (○) MCM-48-(240); (●) MCM-48-(400); (□) MCM-48-(480); (▼) MCM-48-(600).

lower (up to 20%) than the pore volumes calculated from the nitrogen adsorption isotherms using the BJH model, but decrease comparably with increasing compression pressure.

The adsorption isotherms of benzene, cyclohexane, and *n*-heptane onto the six different MCM-48 samples are shown in Figures 8, 9, and 10, respectively. All isotherms are type IV with no hystereses (the desorption points were omitted for clarity) according to the IUPAC classification, with a steep increase between $p/p_0 = 0.15$ and 0.2. According to the differences in surface tension and the molecular volume of the adsorbates, the capillary condensation takes place at varying relative pressures for the same pore diameter. Therefore, capillary condensation was observed at $p/p_0 = 0.20$, 0.18, and 0.16 for cyclohexane, benzene, and *n*-heptane, respectively. The height of the step is determined by the pore volume available in each sample. The last nearly linear part of the isotherm is suggested to be due to adsorption on the outer surface of the small MCM-48 particles and their interparticular voids.[18]

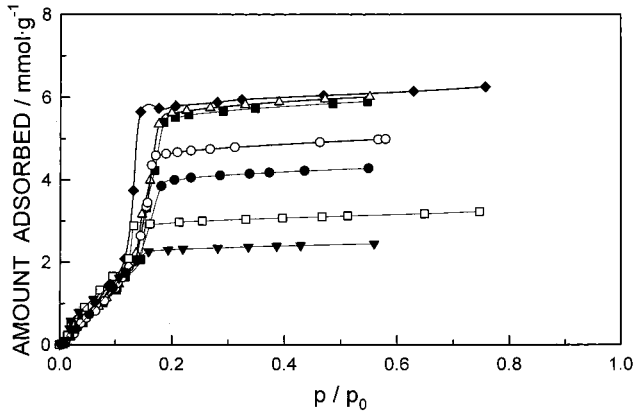

Figure 10. *n*-Heptane adsorption isotherms at 21 °C on MCM-48: (◆) uncompressed sample; (■) MCM-48-(20); (△) MCM-48-(80); (○) MCM-48-(240); (●) MCM-48-(400); (□) MCM-48-(480); (▼) MCM-48-(600).

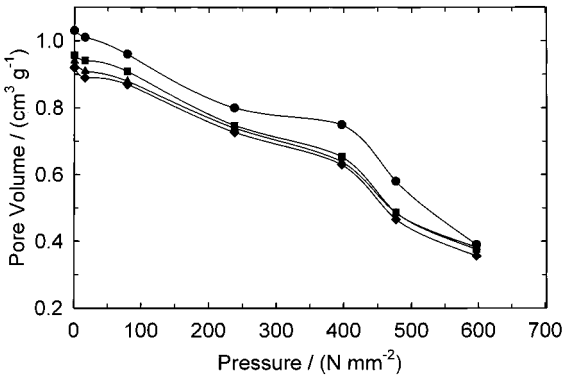

Figure 11. Comparison of the pore volumes of pelletized MCM-48 materials calculated from the adsorption isotherms of nitrogen (●), benzene (■), *n*-heptane (▲), and cyclohexane (◆).

In the low-pressure region, the isotherms otained with the same adsorptive are similar for all samples with the exception of the isotherms of MCM-48-(480) and MCM-48-(600), which are typically slightly more bent toward the pressure axis. As a result of the higher polarity, the benzene isotherms are of the Langmuir type in the low-pressure region (Figure 8), while the *n*-heptane isotherms show a Henry-type behavior owing to the low polarity of *n*-heptane (Figure 10).

With increasing pelletizing pressure, the total adsorption capacity of benzene (Figure 8) decreases from 10.2 mmol g^{-1} for the uncompressed material to 3.3 mmol g^{-1} for MCM-48-(600). This 60% decrease of the total adsorption capacity was also observed with *n*-heptane and cyclohexane. Only a 30% decrease is found after compression with 400 N mm^{-2}.

In Figure 11, the results of the different adsorption experiments are compared by displaying the pore volumes calculated from the amount adsorbed assuming the adsorbed phase has the same density as the liquid phase at adsorption temperature (Gurvich rule).[19] The pore volumes calculated from the adsorp-

tion of organic vapors are consistently smaller than those calculated from the nitrogen isotherm using the BJH model, although the amount adsorbed was extrapolated to $p/p_0 = 0.95$. The deviation increases in the order benzene, *n*-heptane, and cyclohexane. Similar discrepancies were also observed by Branton et al.[20] Possible differences in molecular packing account for a uncertainty in the adsorbed phase density, which was taken as the bulk liquid density at the adsorption temperature. These findings illustrate the difficulty in arriving at a definitive evaluation of the pore volume, even in the case of a model mesoporous adsorbent like MCM-41 or MCM-48.[21]

Discussion

In contrast to the hexagonal phase, MCM-41, the cubic phase MCM-48 has gained less attention, mainly due to the lack of a reliable synthesis procedure. But, once mastered, the synthesis of MCM-48 is as reproducible and reliable as the MCM-41 synthesis.[2,4] As evident from the powder X-ray diffraction patterns (Figure 1) and the results of nitrogen adsorption isotherms (Table 1), the synthesis of MCM-48 can be easily upscaled to produce about 150 g of high-quality material in a 5 L autoclave. The formation of well-ordered MCM-48 occurs via phase transformation from an intermediate phase, which is a disordered three-dimensional arrangement. According to Xu et al., the phase transformation occurs in the order H → L → MCM-48, where the letters H and L designate the tubular and lamellar mesophases, respectively.[4]

Condensation of silanol groups as observed by ^{29}Si MAS NMR (Figure 2) is one of the driving forces triggering the phase transformation and, hence, the MCM-48 formation. Similar results were found by Huo et al.,[22] who investigated the formation of MCM-41 using X-ray diffraction and ^{29}Si MAS NMR. In contrast to the formation of the MCM-48 structure, the characteristic pattern of the MCM-41 phase is already recognizable 10 min after mixing of the synthesis gel. Further crystallization only results in intensity enhancement of the X-ray reflections. This indicates that the hexagonal structure of MCM-41 is already prearranged in the synthesis gel. The MCM-48 material synthesized in this study is characterized by a high BET surface area of 1300 $m^2\ g^{-1}$ and a large pore volume of 1.03 $cm^3\ g^{-1}$. The high pore volume is responsible for the exceptional high loadings of benzene, cyclohexane, and *n*-heptane that exceed 0.7 kg/kg. These result confirm the superior quality of the MCM-48 material synthesized in this study.

In studying the dynamics of a fixed-bed adsorption column, it is convenient to consider the response of an initially free column to a step change in adsorbate concentration. The response to such a step input is commonly called the breakthrough curve (Figures 5−7). The answer to a perturbation in the feed composition results in a mass transfer zone or concentration front, which propagates through the column with a characteristic velocity. The general nature of the mass transfer zone is determined entirely by the equilibrium isotherm, although the shape of the concentration profile may be modified by kinetic effects.[23] Therefore, the general form of the breakthrough curve can be directly derived from the adsorption isotherm. In the case of isotherms with an inflection point, viz. type 2 or type 4 according to the IUPAC classification, the equilibrium is favorable at low concentrations, which results in a shock profile of the respective part of the breakthrough curve. In the region of capillary condensation, the equilibrium is unfavorable, leading to a dispersive front. At high concentrations, the equilibrium is again favorable, resulting in a shock front. In the low-pressure region, the adsorption isotherms of benzene, cyclohexane, and *n*-heptane are almost identical (with the exception of MCM-48-(480) and MCM-48-(600)). Therefore, only slight differences are found in the respective breakthrough curves. The length and the slope of the plateau shown in Figures 5−7 is accordingly determined by the height and the slope, respectively, of the step in the adsorption isotherm. With the adsorption kinetics being largely comparable, partial pore blocking resulting in diffusional limitations can be ruled out. Differences in the initial part of the breakthrough curves are presumably due to differences in the number of adsorption sites available, as expressed by the decline of the surface area, which was also observed in the respective adsorption isotherms. Although the pore volumes determined by the adsorption of subcritical organic vapors are systematically lower than the ones calculated from the nitrogen adsorption data (Table 2 and Figure 11), these results most likely do *not* imply limited excess to the MCM-48 channel system for the substantially larger hydrocarbons. The pore volume V_p (N_2) is calculated from the nitrogen desorption isotherm using the BJH formalism, while the pore volumes were calculated from hydrocarbon breakthrough curves and adsorption isotherms employing the Gurvich rule. Therefore, the observed differences might be due to the different calculation procedure and/or the uncertainty in the adsorbed phase density. Considering the small pore diamater of 2.3 nm, only three to four molecules of the large organics used are needed to span that distance. The isothems can also be explained by adsorption of the organic molecules at the channel wall and subsequent filling of the entire space without condensation, which would also result in a steep rise of the adsorption isotherm due to the favorable adsorption potential. However, the adsorbed phase would than exhibit a lower density than the bulk liquid.

For industrial application of mesoprous molecular sieves, shaping of the powders obtained from the upscaled synthesis is essential to minimize the pressure drop in reactors or adsorption columns. Application of external pressure to MCM-48 powders to form pellets results in a significant loss of adsorption capacity for N_2 and organic subcritical vapors. While the BET surface area is reduced by about 20% from MCM-48 to MCM-48-(400), the pore volume decreases to about 40% of the value of the unpressed material (Table 1), although the pore diameter as determined from the same sorption measurements was not affected by the pelletizing pressure. Keeping in mind that the underlying model used for their calculation limits the accuracy of these numbers, coming up with a reasonable model required further studies with other adsorbates with different sizes. Adsorption of organic vapors such as benzene, cyclohexane, and *n*-heptane, which differ in polarity and kinetic diameter, also shows a decrease of the total adsorption capacity by about 30% with an increase of pelletizing pressure to 400 N mm^{-2}. Similar effects were observed forming MCM-41 pellets applying pressures up to 320 N mm^{-2}. This has been explained by blocking of some pores most probably by other particles of the same material.[12] As a result, the overall specific surface area and the pore volume are reduced, while the average pore diameter is constant. Nevertheless, while this model might be acceptable for MCM-41 with its one-dimensional channel system, blocking of some pores of the three-dimensional MCM-48 structure seems difficult to achieve unless one assumes an eggshell-type catalyst pellet, where the MCM-48 channels of the inner-sphere particles of the pellets are totally blocked by other particles in the outer sphere.

A more likely model is the irreversible destruction of some MCM-48 particles under pressure application which are no

longer accessible for larger molecules such as benzene and *n*-heptane or even nitrogen. Such a model is supported by the powder X-ray diffraction patterns, which decrease in quality with increasing pelletizing pressure. Careful milling (no additional structural loss has been detected) of the pelletized MCM-48-(600) did not result in an increase of the nitrogen adsorption capacity. Therefore, the particle alteration seems irreversible.

In comparison to MCM-41, which exhibits a pore volume of 0.2 $cm^3\ g^{-1}$ (25% of the parent material) and a BET surface of 330 $m^2\ g^{-1}$ after application of 224 N mm^{-2},[24] the MCM-48 materials tested in our study are more stable. A decrease of the pore volume to one-quarter of the parent material is only obtained after application of 600 N mm^{-2}. This is most likely due to the three-dimensional arrangement of the pore system, which together with a higher wall thickness may result in a higher stability of the MCM-48 system. Nevertheless, MCM-48 shows an inferior mechanical stability compared to other adsorbents and catalysts such as zeolites, silica, and alumina,[25,26] which may result from its large porosity and the absence of a stabilizing crystal structure.

Conclusions

The adsorption and breakthrough behavior of benzene, cyclohexane, and *n*-heptane confirm a considerable alteration of the pore structure of MCM-48 by applying an external force. Up to a pressure of 400 N/mm^2, the XRD diffraction patterns are roughly unchanged, while the adsorption capacity calculated from both the nitrogen and subcritical organics adsorption indicate a 30% decrease of the pore volume. The application of higher pressures up to 600 N/mm^2 essentially destroys the pore structure, as evident from the poor XRD patterns and a 3-fold decrease of the adsorption capacity. However, the pore diameter of ca. 2.3 nm is generally not affected by the compression. Therefore, the reduced adsorption capacity is assumed to be due to destruction of less stable particles. The mechanical stability of MCM-48 has been found to be larger than that of MCM-41, which is a consequence of its three-dimensional pore structure and/or larger wall thickness.

Finally, it has been shown that the synthesis of high-quality MCM-48 can be easily upscaled, which is a prerequisite for industrial use of this material. However, care must be taken not to alter the material by the shaping process, which might result in a significant structural degradation and, hence, a significant loss of adsorption capacity.

Acknowledgment. Financial support of this work by Deutsche Forschungsgemeinschaft (DFG) and Fonds der Chemischen Industrie is gratefully acknowledged. M.H. thanks Prof. J. Weitkamp for continuous support.

References and Notes

(1) Corma, A. *Chem Rev.* **1997**, *97*, 2373.

(2) Hartmann, M.; Bischof, C. In *Mesoporous Molecular Sieves 1998*; Bonneviot, L., Béland, F., Danumah, C., Giasson, S., Kaliguine, S., Eds.; Studies in Surface Science and Catalysis, Vol. 117; Elsevier: Amsterdam 1998; pp 249−257.

(3) Romero, A. A.; Alba, M. D.; Zhou, W.; Klinowski, J. *J. Phys. Chem. B* **1997**, *101*, 5294.

(4) Xu, J.; Luan, Z.; He, H.; Zhou, W.; Kevan, L. *Chem. Mater.* **1998**, *10*, 3690.

(5) Vartuli, J. C.; Kresge, C. T.; Roth, W. J.; McCullen, S. B.; Beck, S. B.; Schmitt, K. D.; Leonowicz, M. E.: Lutner, J. D.; Sheppard, E. W. In *Advanced Catalysts and Nanostructured Materials: Modern Synthesis Methods*; Moser, W. R., Ed.; Academic Press: New York, 1996; pp 1−19.

(6) Jentys, A.; Pham, N. H.; Vinek, H.; Englisch, M.; Lercher, J. A. *Microporous Mater.* **1996**, *6*, 13.

(7) Zhao, X. S.; Lu, G. Q. *J. Phys. Chem. B* **1998**, *102*, 1556.

(8) Nguyen, C.; Sonwane, C. G.; Bhatia, S. K.; Do, D. D. *Langmuir* **1998**, *14*, 4950.

(9) Inagaki, S.; Fukushima, Y. *Microporous Mesoporous Mater.* **1998**, *21*, 667.

(10) Rathousky, J.; Zukal, A.; Franke, O.; Schulz-Ekloff, G. *J. Chem. Soc., Faraday Trans.* **1995**, *91*, 937.

(11) Chen, C. Y.; Li, H. X.; Davis, M. E. *Microporous Mater.* **1993**, *2*, 17.

(12) Boger, T.; Roesky, R.; Gläser, R.; Ernst, S.; Eigenberger, G.; Weitkamp, J. *Microporous Mater.* **1997**, *8*, 79.

(13) Hansen, E. W.; Courivaud, F.; Karlsson, A.; Kolboe, S.; Stöcker, M. *Microporous Mesoporous Mater.* **1998**, *22*, 309.

(14) Long, Y.; Xu, T.; Sun, Y.; Dong, W. *Langmuir* **1998**, *14*, 6173.

(15) Jänichen, J.; Busio, H.; Hintze, M.; Stach, H.; van Hooff, J. H. C. In *Progress in Zeolite and Microporous Materials*; Chon, H., Ihm, S.-K., Uh, Y. S., Eds.; Studies in Surface Science and Catalysis, Vol. 105; Elsevier: Amsterdam, 1997; pp 1731−1738.

(16) Jänichen, J.; Stach, H.; Busio, M.; van Wolput, J. H. M. C. *Themochim. Acta* **1998**, *312*, 33.

(17) Ciesla, U.; Schüth, F. *Microporous Mesoporous Mater.* **1999**, *27*, 131.

(18) Van der Runstraat, A.; Kamp, J. A.; Stobbelaar, P. J.; van Grondelle, J.; Krijnen, S.; van Santen, R. A. *J. Catal.* **1997**, *171*, 77.

(19) Gurvich, L. *J. Phys. Chem. Russ.* **1915**, *47*, 805.

(20) Branton, P. J.; Hall, P. G.; Sing, K. S. W. *Adsorption* **1995**, *1*, 77.

(21) Branton, P. J.; Hall, P. G.; Treguer, M.; Sing, K. S. W. *J. Chem. Soc., Faraday Trans.* **1995**, *91*, 2041.

(22) Huo, Q.; Margolese, D. I.; Ciesla, U.; Demuth, D. G.; Feng, P.; Gier, T. E.; Siegler, P.; Firouzi, A. I.; Chmelka, B. F.; Schüth, F.; Stucky, G. D. *Chem Mater.* **1994**, *6*, 1176.

(23) Ruthven, D. M. *Principles of Adsorption and Adsorption Processes*; Wiley-Interscience: New York, 1984.

(24) Gusev, V. Y.; Feng, X.; Bu, Z.; Haller, G. L.; Brien, J. A. O. *J. Phys. Chem.* **1996**, *100*, 1985.

(25) Bosacek, V.; Dubinin, M. M.; Kadlets, O.; Murdmaa, K. O.; Navratil, V. *Dokl. Chem.* **1967**, *174*, 305.

(26) Gregg, S. J.; Langford, J. F. *J. Chem. Soc., Faraday Trans. 1* **1977**, *73*, 747.